PBPC ISSN 2674-9432
Qualis A3 CAPES 2021-2024 | DOI - Crossref | Latindex | Indexado no Google Acadêmico

THE CRUCIALITY OF THE 1, 2, 4-TRIOXANE RING IN THE BIOLOGICAL ACTIVITIES OF ANTICANCER ARTEMISININS: AN EXPERIMENT FOR CHEMICAL EDUCATION AT DIFFERENT LEVELS

Marcos Daniel G. Pizon[1], Márcio de Souza Farias[2], Antonio Florêncio de Figueiredo[3], Ana Cecília B. Pinheiro[4], Marcos Antonio B. dos Santos[5], Andréia de Lourdes R. Pinheiro[6], Fábio dos Santos Gil[7], Heriberto Rodrigues Bintencourt[8], José Ciríaco Pinheiro[1,9]*

https://doi.org/10.36557/2674-9432.2026v5n3p319-342
Artigo recebido em 6 de Março e publicado em 6 de Maio de 2026

ARTIGO ORIGINAL

RESUMO

No experimento proposto, artemisinina e derivados (artemisininas), com e sem a ponte endoperóxido (R-O-O-R'), são investigados através do potencial eletrostático molecular (MEP), dos orbitais moleculares (OMs) e de suas interações com os receptores biológicos transferrina e heme objetivando a compeensão de aspectos da interação com os dois receptores biológicos e deslindar a importância do anel 1, 2, 4-trioxano nas atividades antitumorais dessa classe de compostos em células HepG2. O padrão dos mapas de MEP obtidos com o método teórico B3LYP/conjunto de base 6-31G** indica que as artemisininas portadoras do anel 1, 2, 4-trioxano são ativas contra o câncer de fígado HepG2 e podem sofre ataques eletrofílicos pelos receptores transferrina e heme na região da ponte endoperóxido (C3-O2-O1-C12a). O posicionamento dos OMs nos átomos das artemisininas suportam a ancoragem dos receptores transferrina e heme no processo de interação ligante-receptor. A investigação do acoplamento ligante-receptor evidenciou que as artemisininas na interação com a transferrina e heme apresentam $d(O1Fe^{2+}) < d(O2Fe^{2+})$, e essas distâncias aumentam com a atividade biológica (IC_{50}). A comparação de $d(O1Fe^{2+})$ e $d(O2Fe^{2+})$ para transferrina e heme evidencia distâncias maiores na interação com transferrina. Finalmente, a investigação com MEP, OMs e interação ligante-receptor indica a relevância do anel 1,2,4-trioxano na atividade anticâncer das artemisininas.

Palavras-chave Artemisininas; Anel 1, 2, 4-trioxano; Potencial eletrostático molecular; Orbital molecular; Interação ligante-receptor.

ABSTRACT

In the proposed experiment, artemisinin and its derivatives (artemisinins), with and without the endoperoxide bridge, (R-O-O-R'), are investigated through molecular electrostatic potential (MEP), molecular orbitals (MOs), and their interactions with the biological receptors transferrin and heme, aiming to understand aspects of the interaction with the two biological receptors and to clarify the importance of the 1,2,4-trioxane ring in the antitumor activities of this class of compounds in HepG2 cells. The pattern of MEP maps obtained with the theoretical method B3LYP/6-31G** basis set indicates that artemisinins carrying the 1,2,4-trioxane ring are active against HepG2 liver cancer and may undergo electrophilic attacks by transferrin and heme receptors in the endoperoxide bridge region (C3-O2-O1-C12a). The positioning of MOs on artemisinin atoms supports the anchoring of transferrin and heme receptors in the ligand-receptor interaction process. Investigation of ligand-receptor, molecular docking, showed that artemisinins interacting with transferrin and heme exhibit $d(O1Fe^{2+}) < d(O2Fe^{2+})$, and these distances increase with biological activity (IC_{50}). Comparison of $d(O1Fe^{2+})$ and $d(O2Fe^{2+})$ for transferrin and heme shows greater distances in the interaction with transferrin. Finally, investigation with MEP, MOs, and ligand-receptor interaction indicates the relevance of the 1,2,4-trioxane ring in the anticancer activity of artemisinins.

Keywords: Artemisinins; 1,2,4-trioxane ring; Molecular electrostatic potential; Molecular orbital; Ligand-receptor interaction.

Instituição afiliada
[1]Laboratório de Química Teórica e Computacional (LQTC), Universidade Federal do Pará, Belém, PA, Brasil
[2]Colégio Estadual Paes de Carvalho, Belém, PA, Brasil
[3]Instituto Federal de Educação, Ciência e Tecnologia, Castanhal, PA, Brasil
[4]Fundação Santa Casa de Misericórdia do Pará, Belém, PA, Brasil
[5]Universidade Estadual do Pará, Belém, PA, Brasil
[6]Centro Educa Mais Padre José Bráulio Souza Ayres, São Luís, MA, Brasil
[7]Escola Estadual Rodrigues Pinagé, Belém, PA, Brasil
[8]Laboratório de Sínteses (LabSínt), Universidade Federal do Pará, Pará, PA, Belém, Brasil
[9]Instituto Amazônia dos Saberes, São Luís, MA, Brasil

Autor correspondente*:* José Ciríaco Pinheiro ciriaco@ufpa.br

1 INTRODUCTION

Cancer is the name given to a group of devastating diseases characterized by the uncontrolled growth and multiplication of abnormal cells, capable of invading nearby structures and spreading to various regions of the body. According to the literature, the disease is among the leading causes of death for people aged 30 to 69 in 177 countries worldwide (Bray *et al.,* 2024). The appearance of abnormal cellular features in this disease reflects altered patterns of gene expression due to mutations in the DNA of these cells (Rosenberg *et al.,* 2021; Xu *et al.,* 2021).

Among the strategies used in cancer treatment is chemotherapy with drugs that act specifically on cancer cells. However, the widespread use of this strategy has encountered a very difficult barrier because these cells, being very similar in numerous aspects, make it difficult to identify general and exploitable biochemical differences between them (Xu *et al.,* 2021; Haber & Fearon, 1998). Thus, the ability to cause specific and highly potent cancer cell death is one of the most sought-after aspects in drugs designed for cancer chemotherapy (Xu *et al.,* 2021; Efferth *et al.*, 2005).

The task of great motivation in research on natural sources, particularly plants used in traditional folk medicines, has proven successful (Wall & Wani, 1996; Wen *et al.,* 2024). Among the plants used is Artemisia annuar L. (qinghao), an herb that has been commonly used in traditional Chinese medicine, carrying the active principle artemisinin (qinghaosu) and its most common derivatives (artemether, artesunate and artether) used in the treatment of falciparum and vivax malaria (Prince *et al.,* 1998; Wani *et al.,* 2021; Gu *et al.,* 2024). Artemisinin derivatives are transformed into the active metabolite, didroartemisinin, and its use has been an integral part of the fight against malaria in most modern treatments (Cardoso *et al.,* 2008; Wani *et al.,* 2021).

Artemisinin is a trioxane sesquiterpene lactone whose endoperoxide bridge is essential for its antimalarial, anticancer, leishmanicidal, and antifungal activity (Avery *et al.,* 2003; Wani *et al.,* 2021; Khanal, 2021). In the last two decades, the sensitivity to artemisinin and its first-generation derivatives – artesumate, artemether, arteether, and artelinate – has been evaluated in a number of tumor cells. Artemisinin and its derivatives have been found to exhibit cytotoxicity to mammary cells in the nanomolar to micromolar concentration range (Opsenica & Solaja, 2009; Jana *et al.,* 2027; Ma *et*

al., 2021). Also, low concentrations of these compounds exhibit cytotoxicity in leukemia cells, colon cancer, lung cancer, and renal cancer (Efferth *et al.,* 2001; Ma *et al.,* 2021), thyroid cancer (Rinner *et al.,* 2004), cervical cancer, uterine cancer, and ovarian cancer (Chen *et al.,* 2003; Ma *et al.,* 2021).

Mammalian cells, both normal and cancerous, use the protein transferrin to capture iron ions. This protein, bound to ferrous ions, forms holotransferrin, which is transported into cells via a specific receptor known as the transferrin receptor (Andrews, 2000). On the other hand, experiments demonstrate that artemisinin derivatives covalently linked to holotransferrin are transported together with the protein into the cells (normal and tumor) through an endosome formation process mediated by the specific transferrin receptor. Inside the endosome, the endoperoxide bridge of the artemisinin derivative can react with the iron released by transferrin and produce toxic free radicals (Lai *et al.,* 2006). These radical species are highly reactive and responsible for the death of different cell types. Among the deleterious effects of free radicals are: enzyme inactivation; degradation of structural proteins; destruction of membranes; apoptosis; and others.

Recent results reported in the literature show that the administration of artemisinins targeted to mitochondria, together with ligand-mediated modulation of molecule conformation, significantly increases their anticancer activity and results in greater binding affinity to heme and Fe ions (Dan-Dan *et al.,* 2025).

In this investigation, the anticancer behavior of artemisinin and derivatives (artemisinins) (Liu *et al.,* 2005), with and without endoperoxide bridge, (R-O-O-R'), is investigated through molecular electrostatic potential, molecular orbitals and their interactions with the biological receptors transferrin and heme (the objective is not to investigate the mechanism of action of the compounds, but aspects of the interaction with the two biological receptors). The results obtained will support the discussion and elucidation of the importance of the 1,2,4-trioxane ring in the anticancer biological activities of this class of compounds in HepG2 cells and will be reported and made available as a Theoretical Chemistry/Computational Chemistry experiment accessible to different levels of Chemistry Education.

2 EXPERIMENT OVERVIEW

The theoretical approaches shown in Figure 1 were used in the experiment; and for their design, a literature review was previously conducted on the topic of human hepatocellular carcinoma (HepG2)/artemisinins, considering the biological activities tested and the target biological receptor.

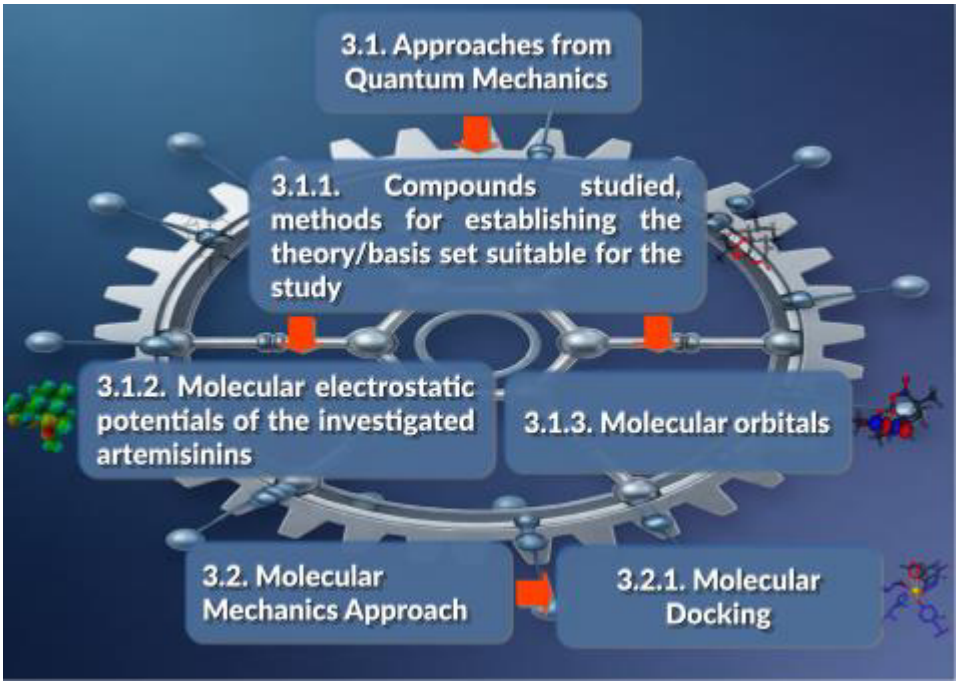

Figure 1. Theoretical approaches used in the experiment.

Information on artemisinins with different IC_{50} values for HepG2 allowed the design and execution of the experiment with the compounds in Figure 2 (See Section 3. The Detailed Experiment), with the transferrin and heme receptors, Figure 3I e 3II (See Section 3.

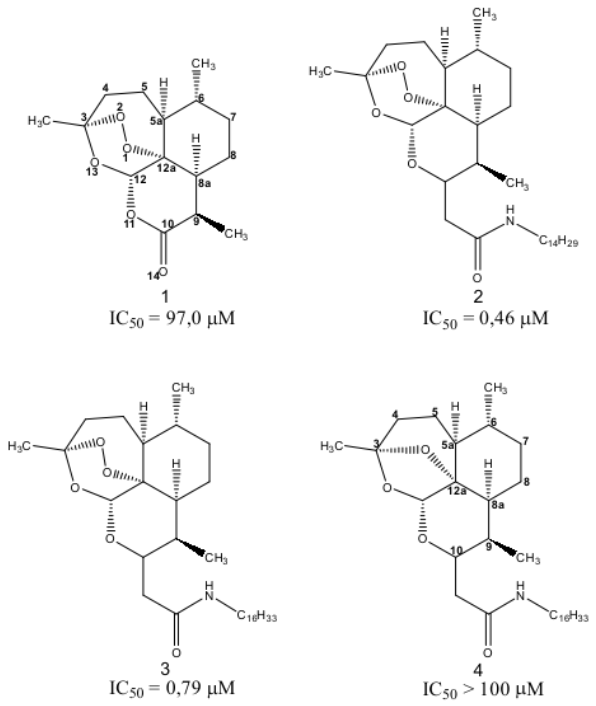

Figure 2. 2D structure of artemisinin (**1**) and derivatives (**2**, **3**, and **4**) biologically assayed against HepG2 cancer

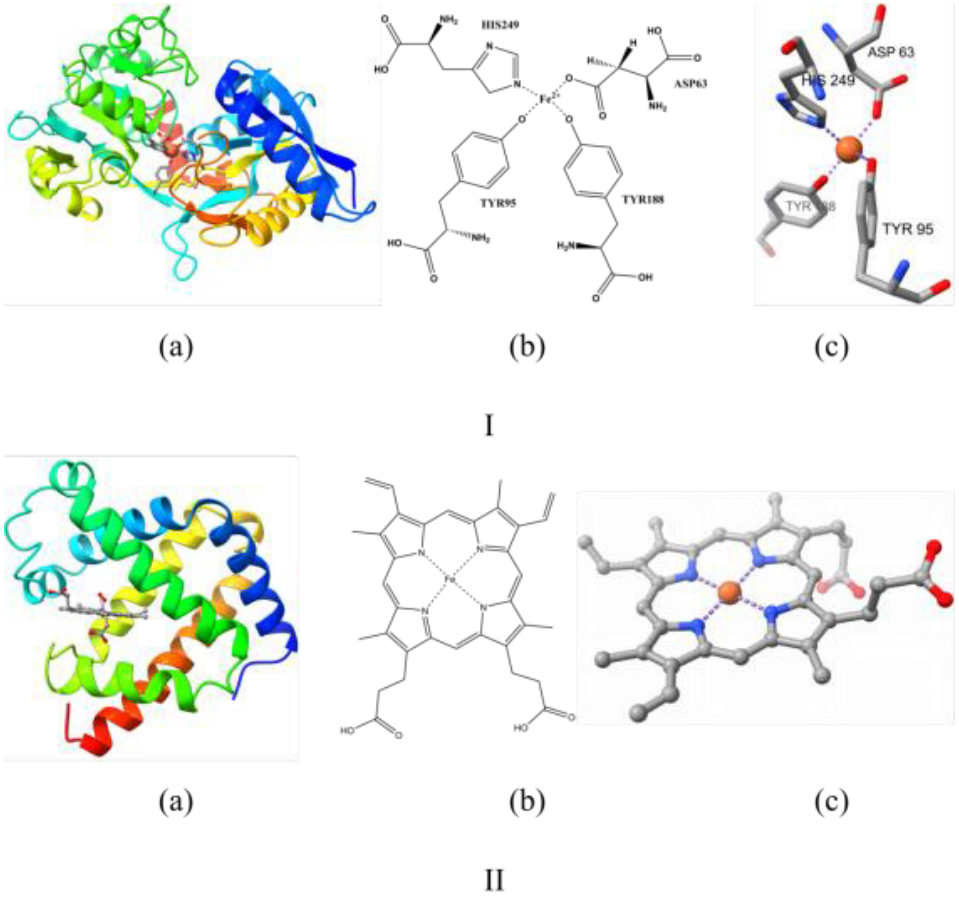

Figure 3. (I) Transferrin protein (a) obtained from the Protein Data Bank (PDB-RCSB), code 1a8E, and 2D (b) and 3D (c) structures selecting the iron-containing fragment

coordinated with four amino acid linkages: two (2) tyrosines, one (1) histidine, and one (1) aspartate, and (II) myoglobin (a) obtained from the Protein Data Bank (PDB-RCSD), code 1A6M, 2D (b) and 3D (c) structures of heme containing the histidine residue.

The Detailed Experiment), being considered in the investigation phase of interactions with the biological target. The 3D structure of artemisinin was retrieved from the Protein Data Bank (PDB) crystallographic database, CCD code – 691593, and its complete optimization was performed with different theoretical approximations/basis sets, namely: HF/3-21G, HF/6-31G, HF/63-1G*, HF/6-31G**, B3LYP/3-21G, B3LYP/6-31G, B3LYP/6-31G*, B3LYP/6-31G**, AM1, and PM3, and the geometric parameters were compared with experimental data from the literature, which allowed the selection of the most suitable theoretical approximation/basis set to describe the most stable conformation of artemisinin, which was used to construct the 3D structures of the other investigated compounds, which were also subjected to complete optimization. The most stable conformations of the investigated compounds were used to calculate the molecular electrostatic potentials, whose maps are shown in Figure 4 (See Section 4. Results and Discussion), while the molecular orbitals shown in Figure 5 (See Section 4. Results and Discussion), and the interactions with transferrin and heme receptors shown in Figures 6 and 7 (See Section 4. Results and Discussion), respectively.

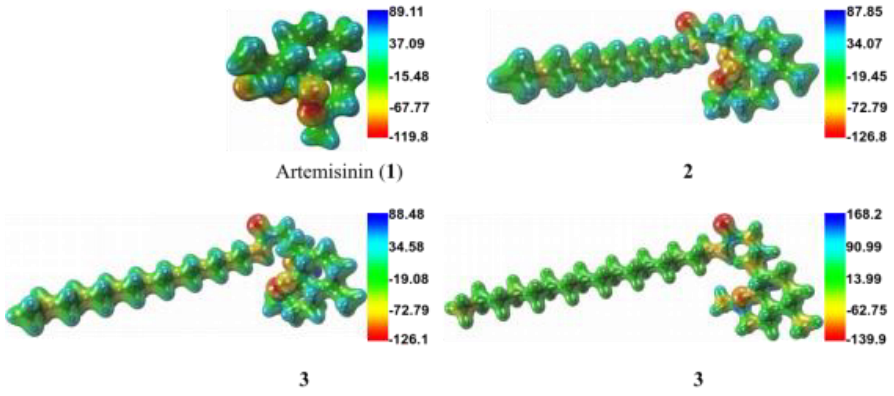

Figure 4. MEP (kcal/mol) maps for artemisinin (**1**) and derivatives (**2**, **3**, e **4**) biologically assayed against HepG2 cancer.

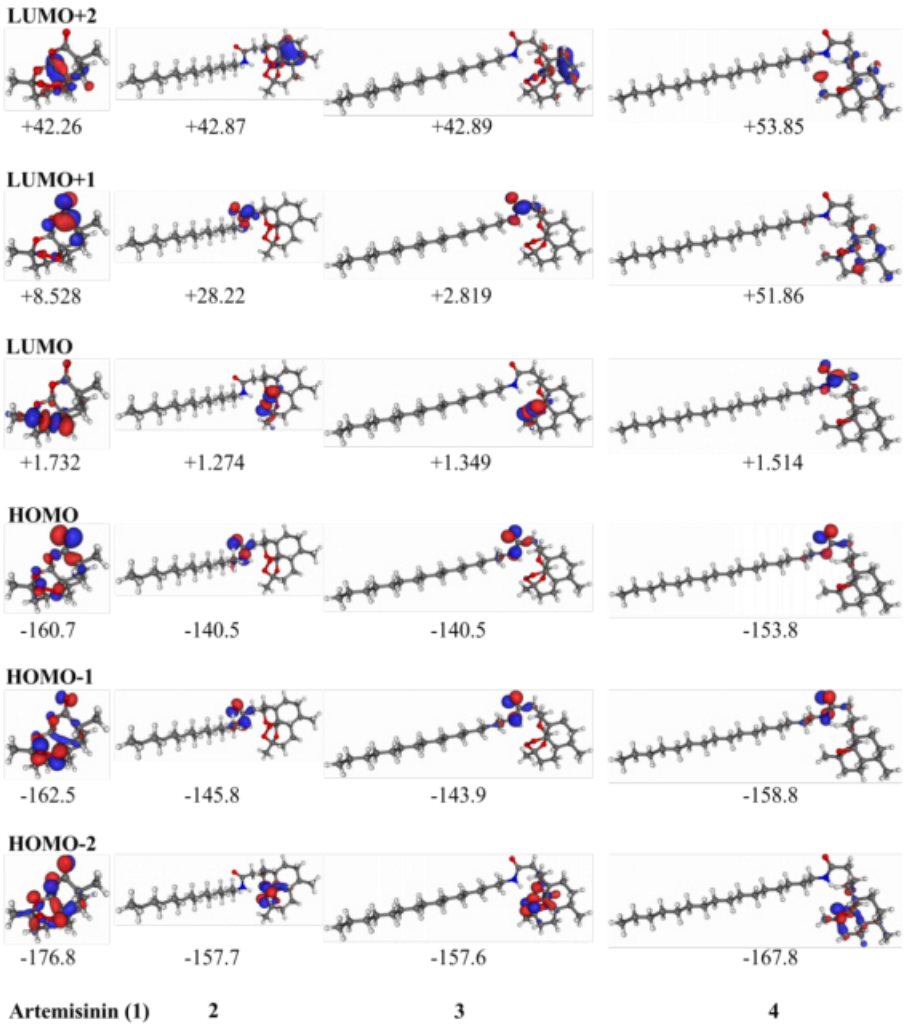

Figure 5. Molecular orbitals (LUMO+2, LUMO+1, LUMO, HOMO, HOMO-1, HOMO-2) and orbital energies (kcal/mol) for artemsisinin (**1**) and derivatives (**2**, **3**, and **4**) biologically assayed against HepG2 cancer.

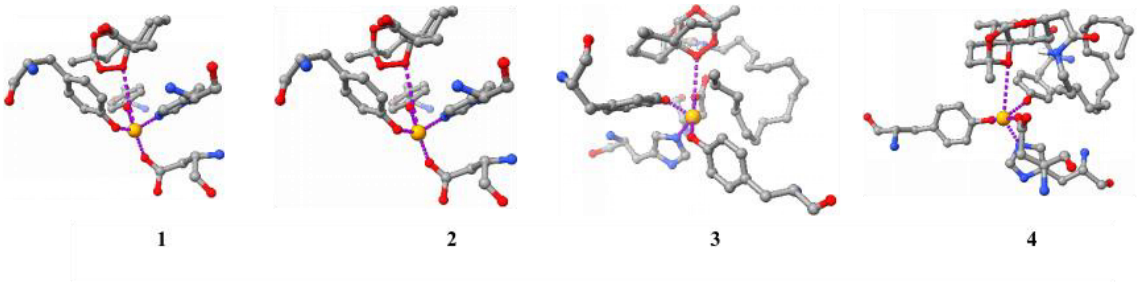

Figure 6. Interaction between artemisinin (**1**) and derivatives (**2**, **3**, and **4**), biologically tested against HepG2 cancer, with the transferrin receptor. Atoms and colors: C (gray); N (blue); O (red); and Fe (orange).

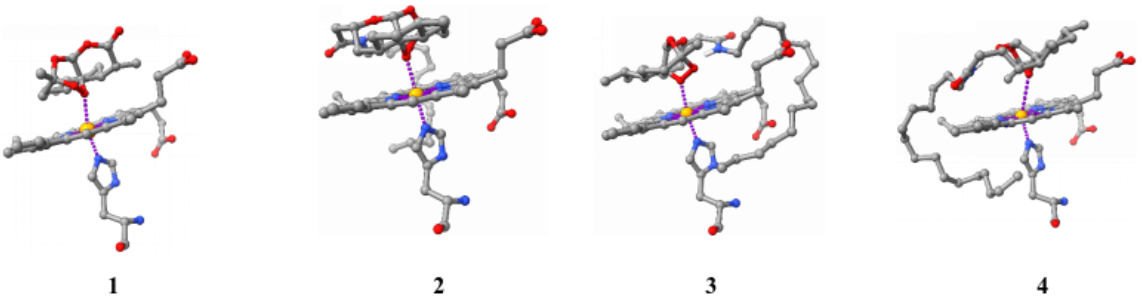

Figure 7. Interaction between artemisinin (**1**) and derivatives (**2**, **3**, and 4), biologically tested against HepG2 cancer, with the heme receptor. Atoms and colors: C (gray); N (blue); O (red); and Fe (orange).

3 THE DATAILED EXPERIMENT

3.1 APPROACHES FROM QUANTUM MECHANICS

3.1.1 COMPOUNDS STUDIED, METHODS FOR ESTABLISHING THE THEORY/BASIC SET SUITABLE FOR THE STUDY

Figure 2 shows the 2D structures of the studied compounds **1** (IC50 = 97.0 µM), **2** (IC_{50} = 0.46 µM), **3** (IC_{50} = 0.79 µM), and **4** (IC_{50} > 100 µM) (Liu *et al.,* 2005). The numbering adopted is the same as in the literature (Avery *et al.,* 2003). The 3D structure of artemisinin, coded CCDC-691593, extracted from the crystallographic database (Allen, 2002) with the Chimerax-DockPrep software (Meng *et al.,* 2023) was subjected to full optimization with different levels of the theory/basis set, namely: HF/3-216, 6-31G, 6-31G*, and 6-31G** (Roothann, 1951; Hehre *et al.,* 1986); B3LYP/3-21G, 6-31G, 6-31G*, and 6-31G** (Lee *et al.,* 1988; Becke, 1993); AM1 (Dewar, 1985); and PM3 (Wu *et al.,* 2013) available in the Gaussian 98 software package (Frisch *et al.,* 1998). The geometric parameters obtained were compared with experimental data from the literature (Leban *et al.,* 1988; Lisgarten *et al.,* 1988), and the most suitable theoretical method/basis set to describe the most stable conformation of artemisinin was selected, which was then used in the construction of the 3D structures of its derivatives and subjected to full optimization; with the most stable conformations of artemisinin and derivatives being important for the following steps of the experiment. Continuing the procedure for obtaining the most stable conformations of the compounds, the 3D structure of artemisinin after full optimization with different theory/basis set was visualized, for the purpose of extracting corresponding geometric parameters with

Molden 6.0 software (Schaftenaar & Noordik, 2000), converted with the help of OpenBabel software (O'Boyle *et al.,* 2011) and used to build the 3D structures of the derivatives with HyperChem software (HyperChem, Inc., 2008), which were also converted with OpenBabel software into inputs of the Gaussian 98 program package for the full optimization step.

3.1.2 MOLECULAR ELECTROSTATIC POTENTIALS OF THE INVESTIGATED ARTEMISININS

The most stable conformations of artemisinin and derivatives in the theoretical approximation/basis set selected as the most suitable were applied in the calculations of the electrostatic potentials of each molecule, $V(\vec{r})$; here it is worth remembering that physically the electrostatic potential means the description of the surroundings of a molecule and, with it, one seeks the main key characteristics that determine the occurrence or not of a recognition of one molecule (drug) by another (receptor). This approximation of Quantum Mechanics proves to be an effective means of analyzing and elucidating the recognition processes (Politzer & Truhlar, 1981; Politzer *et al.,* 1985; Oliveira *et al.,* 2021).

In the experiment performed, the $V(\vec{r})$ produced by the molecule, having an electron density function $(\vec{r})$ at any point $\vec{r}$, was rigorously calculated by eq. (1), given below (Politzer & Murray, 2021; Pizon *et al.,* 2024):

$$V(\vec{r}) = \sum_{A} \frac{Z_A}{|\vec{R}_A - \vec{r}|} - \int \frac{\rho(\vec{r}')d\vec{r}'}{|\vec{r}' - \vec{r}|} \quad (1)$$

where Z_A is the charge on the nucleus A, located in $\vec{R}_A$. The first term on the right-hand side of eq. (1) represents the positive contribution of the nuclei and the second term characterizes the negative effect of the electrons. The MEP calculations were developed using electron density.

3.1.3 MOLECULAR ORBITALS

In processes involving the interaction between small molecules and biological receptors, molecular orbitals frequently contribute to the biological activity of the molecules through reactions involving charge transfer. Therefore, it becomes relevant to qualify molecular orbitals as one of the important properties in the mechanism of action of these molecules. In this experiment, each molecular orbital was constructed

using the linear combination of atomic orbitals (LCAO MO) approximation (Roothann, 1951; Blinder, 1965; Pople & Beveride, 1970; Dewar & Kelemen, 1971) through eq. (2):

$$\varphi_i = \sum_{\mu} c_{\mu_i} \psi_{\mu} \quad (2)$$

where c_{μ_i} are the molecular orbital expansion coefficients and ψ_{μ} represents a set of orbitals associated with the component atoms of the molecule.

The MEP and molecular orbital maps were visualized with the Molekel software (Flukiger *et al.,* 2000-2001).

3.2 MOLECULAR MECHANICS APPROACH

3.2.1 MOLECULAR DOCKING

The ligand-receptor interaction (molecular docking) provides detailed information on how the ligand (a small molecule) interacts with the receptor (a macromolecule) in the binding region, providing information for understanding the ligand's biological activity. Additionally, it allows visualization and quantification of how the two molecules interact and the respective interaction. The process begins with the ligand seeking its best docking position in the receptor's active site, generating a number of conformational possibilities to establish the best ligand-receptor anchoring (Stanzione *et al.,* 2021; Araújo *et al.,* 2022; Thomse, 2023; Castro *et al.,* 2023). Molecular recognition (ligand-receptor) involves different stages of conformational accommodation, resulting in the favorable mode of interaction relative to enthalpy and entropy. Furthermore, the processes resulting from this stage can be estimated by eq. (3), through ΔG (Gibbs free energy of binding, ELL), related to Ki (inhibition constant), determined experimentally. Also in eq. (3), ΔH is the enthalpy change, T is the absolute temperature, ΔS is the entropy change, and R is the universal gas constant,

$$\mathrm{G} = \mathrm{H} - \mathrm{TS} = \mathrm{RT}\,\ln \mathrm{K_i} \quad (3)$$

The transferrin receptor (MacGillivray *et al.,* 1988) was extracted from the RCSB-PDB database (Protein Data Bank), code 1A8E, Figure 3Ia, architecture described in the literature (MacGillivray *et al.,* 1988), and the fragment containing iron coordinated with four amino acid linkages was selected, being tyrosines (two), histidine (one), and

aspartate (one). Figures 3Ib and 3Ic show the 2D (3Ib) and 3D (3Ic) structures for the transferrin receptor, respectively.

In turn, the heme receptor (Votjtechovsky *et al.,* 1999) was obtained from the PDB-RCSB, identified with code 1A6M with architecture described in reference (Protein Data Bank), Figure 3IIa. The arrangement for calculating the ligand-receptor interaction considered the presence of the histidine residue under the plane of the porphyrin ring. This histidine unit is usually coordinated perpendicularly to the Fe^{2+} ion through the sp^2 N atom of the imidazole ring, Figures 3IIb and 3IIc, which also show, respectively, the 2D (3IIb) and 3D (3IIc) structures of the heme receptor; This procedure will allow the Fe^{2+} of heme to achieve an approximately hexacoordinated arrangement after the formation of the bonds with artemisinin (**1)** and derivatives (**2**, **3**, and **4**).

To investigate ligand-receptor interaction, the AutoDock software (Godosell *et al.,* 1996) was used, with the Lamarckian Genetic Algorithm, with boxes of dimensions 50 units in each direction for all ligand-receptor interactions; with the coordinates of the Center of Mass (CM) of the ligands positioned according to the coordinates: x = 49.994; y = 50.720; and z = 51.577 for the transferrin receptor, and x = 14.515; y = 27.975; and z = 4.750 for the HEME receptor, with the orientation for each ligand being made above the plane of the Fe^{2+} ion; the number corresponding to 1000 conformations was analyzed. In addition, the ligand-receptor interaction calculations in the most stable conformation of each molecule were performed on a Linux Mint platform with a Phenom FX8320 processor and 8 GB of RAM.

4 RESULTS AND DISCUSSION

4.1 APPROACH THROUGH QUANTUM MECHANICS

4.1.1 SELECTION OF THE THEORETICAL METHOD/BASIS SET USED IN THE INVESTIGATION

Table 1 shows the geometric parameters calculated with different theories/basis sets and experimental data (Leban *et al.,* 1988; Lisgarten *et al.,* 1988) for the 1,2,4-trioxane ring in artemisinin (**1**). According to this table, the bond lengths are, in general, well described at all levels of the theory, however the endoperoxide bridge (C3-O1-O2-C12a) is best described at the B3LYP/6-G1* and B3LYP/6-31G** levels. In addition, all

calculated bond angles are very close to the experimental data (Leban *et al.,* 1988; Lisgarten *et al.,* 1988). For the dihedral angle of the twisted boat conformation (-O1-O2-C3-O13-) adopted in artemisinin (**1**), the theoretical results at all levels show a very good description when compared to the experimental data. A better description of the endoperoxide bridge combined with the good description of the bond angles and the twisted boat conformation, as well as the need for a good description of the bulky substituents with a large number of H atoms in the C10 position (derivatives **2**, **3**, and **4**), led to the definition of the theoretical method/basic set B3LYP/6-31G**, in which a p symmetry function is considered in the basis set for the said atomic species, as the most suitable for the investigation.

Table 1. Theoretical and experimental geometric parameters of the 1,2,4-trioxane ring for artemisinin (**1**)

Geometric parameters	Theoretical approaches/bais set										Experimental	
	HF/ 3-21G	HF/ 6-31G	HF/ 6-31G*	HF/ 6-31G**	B3LYP/ 3-21G	B3LYP/ 6-31G	B3LYP/ 6-31G*	B3LYP/ 6-31G**	AM1	PM3	(Leban *et al.*, 1988)	(Lisgarten *et al*, 1988)
C12a-O1	1.471	1.469	1.429	1.429	1.504	1.499	1.455	1.455	1.468	1.426	1.450(4)	1.462(3)
O1-O2	1.462	1.447	1.390	1.390	1.524	1.524	1.460	1.460	1.289	1.544	1.474(4)	1.469(2)
O2-C3	1.441	1.436	1.396	1.396	1.456	1.452	1.414	1.414	1.447	1.406	1.418(4)	1.416(3)
C3-O13	1.436	1.435	1.408	1.408	1.473	1.473	1.441	1.441	1.427	1.428	1.451(4)	1.445(3)
O13-C12	1.408	1.403	1.376	1.376	1.431	1.426	1.376	1.376	1.416	1.403	1.388(4)	1.380(3)
C12-C12a	1.529	1.529	1.533	1.32	1.532	1.532	1.538	1.539	1.537	1.555	1.528(5)	1.523(2)
C12a-O1- O2	111.3	113.2	112.7	112.7	109.6	111.4	111.6	111.6	113.7	112.2	111.5(2)	111.1(1)
O1-O2-C3	107.1	108.8	109.5	109.5	105.6	107.3	108.2	108.3	112.5	110.3	117.7(2)	108.1(2)
O2-C3-013	107.3	106.8	107.8	107.8	108.2	107.7	108.5	108.5	103.6	104.8	107.1(2)	106.6(2)
C3-O13- C12	115.7	117.3	115.3	115.3	113.2	115.0	114.1	114.1	115.5	116.0	113.6(3)	114.2(2)
O13-C12-C12a	112.1	112.9	112.3	112.2	113.3	113.6	113.3	113.3	113.5	115.2	114.7(2)	114.5(2)
C12-C12a-O1	111.6	110.9	110.6	110.6	112.4	111,7	111.3	111.3	111.1	113.2	111.1(2)	110.7(2)
Dihedral angle (degree)												
C12a-O1-O2-C3	50.3	46.7	48.7	48.7	51.1	48.9	47.9	47.9	47.1	35.6	47.7(3)	47.8(2)
O1-O2-C3-O13	-74.7	-74.9	-73.4	-73.4	-76.6	-73.5	-74.0	-73.0	-77.8	-75.3	-75.5(3)	-75.5(2)
O2-C3-O13-C12	32.3	33.4	31.1	31.1	33.8	35.0	32.9	32.9	42.1	52.7	36.3(4)	36.0(2)
C3-O13-C12-C12a	28.3	25.2	27.4	27.4	29.0	26.3	27.3	27.3	11.4	2.8	24.7(4)	25.3(2)

O13-C12-C12a-O1	-50.9	-49.4	50.1	-50.1	-52.7	-51.2	-51.1	-51.2	-41.8	-40.5	-50.8(4)	-51.3(2)
C12-C12a-O1-O2	10.0	12.5	10.5	10.9	9.60	12.8	11.7	11.7	12.0	20.0	12.2(3)	12.6(2)

4.1.2 MOLECULAR ELECTROSTATIC POTENTIAL MAPS

Figure 4 shows the molecular electrostatic potential maps for artemisinin (**1)** e derivatives (**2**, **3**, and **4)**. According to this figure, artemisinin (**1)** e derivatives (**2**, and **3**) with activity against liver cancer exhibit negative electrostatic potentials, of colors red, yellow, and green (energy range from -126.08 to -15.48 kcal/mol), with more negative contours located on the 1,2,4-trioxane ring (color: red). In this region, artemisinin (**1)** and derivatives (**2**, and **3)** may undergo electrophilic attacks by a macromolecule (biological target, in this case transferrin and heme). In this figure, the most negative electrostatic potential is located on the endopeoxide bridge (C3-O1-O2-C12a), in principle, with the possibility of ligand-receptor interaction occurring. Furthermore, these compounds exhibit a positive electrostatic potential, color blue (energy range from +34.07 to +89.11 kcal/mol). Derivative (**4)** (IC_{50} >100 µM) exhibits a negative electrostatic potential (energy range from -139.9 to -62.75 kcal/mol), with the loss of the endoperoxide bridge and, consequently, of the trioxane ring. Additionally, the distribution of electron density in the trioxane ring in the molecules induces their anticancer activities against HepG2, a perception anchored in the fact that the complexation of artemisinin and its derivatives with transferrin and heme particularly involves the interaction between the peroxide bond, the most negatively charged region in the ligand, and the Fe^{2+} ion, the most positive region in the transferrin (Lai *et al.,* 2006) and heme (Sasaki *et al.,* 2007; O'Neill *et al.,* 2010) receptors. Therefore, as noted above, the presence of a red surface near the trioxane ring suggests that artemisinin and its derivatives possess a reactive site for electrophilic attack and should exhibit anticancer activity. Thus, in the case of an electrophilic attack by the Fe^{2+} ion of transferrin and of heme against an electronegative region of the compounds studied, this attack has a strong preference for occurring through the involvement of the endoperoxide bridge (C3-O2-O1-C12a). The pattern of the MEP maps in Figure 4 is an indication that artemisinin and its derivatives (**2** and **3)** in Figure 2 are active against HepG2 cancer.

4.1.3 MOLECULAR ORBITALS

Figure 5 shows the positioning of the molecular orbitals LUMO+2, LUMO+1, LUMO, HOMO, HOMO-1 and HOMO-2 for artemisinin (**1**) and derivatives (**2**, **3**, and **4)**. According to this figure, the molecular orbitals are positioned as follows: artemisinin (**1**): LUMO+2 on atoms O1, O2, O13, O11, C8, C10, C8a, C8, C7, C6, C5a, and C12a, and exhibits $\varepsilon_{\mathrm{LUMO+2}}$ = +42.26 kcal/mol; LUMO+1 on atoms O1, O2, O11, C12, C10, C9, C8a, and C12a, exhibiting $\varepsilon_{\mathrm{LUMO+1}}$ = +8.528 kcal/mol; LUMO on atoms C1, C2, O11, O14, C10, C3, and 12a, with $\varepsilon_{\mathrm{LUMO}}$ = +1.732 kcal/mol; HOMO mainly on atoms O1, O2, O13, O11, O14, C12, C10, C9, C8a, and C8, with $\varepsilon_{\mathrm{HMO}}$ = -160.7 kcal/mol; HOMO-1, on atoms O1, O2, O13, O11, O14, C3, C5a, C10, C9, C8a, C12a, C5a, C6, and C8a, exhibiting $\varepsilon_{\mathrm{HOMO-1}}$ = -162.5 kcal/mol; and HOMO-2 on atoms O1, O2, O13, O11, C9, O14, C3, C5a, C10, C9 C8a, C12a, C5a, C6, and C8a, with $\varepsilon_{\mathrm{HOMO-2}}$ = - 176.8 kcal/mol; derivative (**2**): LUMO+2 on atoms O1, O2, O13, O11, O14, C5a, C12, C10, and C9, with $\varepsilon_{\mathrm{LUMO+2}}$ = +42.87 kcal/mol; LUMO+1 at atoms outside the trioxane ring region, exhibiting $\varepsilon_{\mathrm{LUMO+1}}$ = +28.22 kcal/mol; LUMO on atoms O1, O2, O13, O11, O14, and C12a, with $\varepsilon_{\mathrm{LUMO}}$ = +1.274 kcal/mol; HOMO at atoms outside the trioxane ring region, exhibiting $\varepsilon_{\mathrm{HOMO}}$ = -140.5 kcal/mol; HOMO-1 at atoms outside the trioxane ring region, with $\varepsilon_{\mathrm{HOMO-1}}$ = -145.8 kcal/mol; and HOMO-2 on atoms O1, O2, O13, O11, O14, C12, C10, and C9, exhibiting $\varepsilon_{\mathrm{HOMO-2}}$ = -157.7 kcal/mol; derivative (**3**): LUMO+2 mainly at atoms O1, C5a, C3, and C10, exhibiting $\varepsilon_{\mathrm{LUMO+2}}$ = +42.89 kcal/mol; LUMO+1 at atoms outside the trioxane ring region, with $\varepsilon_{\mathrm{LUMO+1}}$ = +2.819 kcal/mol; LUMO on atoms O1, O2, C3, C5a, C12a, and O13, with $\varepsilon_{\mathrm{LUMO}}$ = +1.349 kcal/mol; HOMO at atoms outside the trioxane ring region, exhibiting $\varepsilon_{\mathrm{HOMO}}$ = -140.5 kcal/mol; HOMO-1 at atoms outside the trioxane ring region, with $\varepsilon_{\mathrm{HOMO-1}}$ = -143.9 kcal/mol; and HOMO-2 on atoms O1, O2, C3, C5, I2a, and C8a, exhibiting $\varepsilon_{\mathrm{HOMO-2}}$ = -157.6 kcal/mol; and derivative (**4**): LUMO+2 on atoms O1, O2, O13, O11, O14, C12, C10, C9, C8a, and C8, exhibiting $\varepsilon_{\mathrm{LUMO+2}}$ = +53.8 kcal/mol; LUMO+1 on atoms C4, O11, C3, C12, with $\varepsilon_{\mathrm{LUMO+1}}$ = +51.86 kcal/mol; LUMO at atoms outside the trioxane ring region, exhibiting $\varepsilon_{\mathrm{LUMO}}$ = +1.514 kcal/mol; HOMO on atoms O1, O2, O3, C3, O11, and C6, with $\varepsilon_{\mathrm{HOMO}}$ = -153.8 kcal/mol; HOMO-1 on atoms O1, 12a, C3, O13, exhibiting $\varepsilon_{\mathrm{HOMO-1}}$ = -158.8 kcal/mol; and HOMO-2 on atoms O2, O13, O11, O14, C3, C5a, C10, C9, C8a, C12a, C5a, C6, and C8, exhibiting $\varepsilon_{\mathrm{HOMO-2}}$ = -167.8 kcal/mol.

4.2 MOLECULAR MECHANICS APPROACH

4.2.1 MOLECULAR DOCKING

Figure 6 shows the ligand **1**, **2**, **3**, and **4** – receptor (transferrin) interactions. According to this figure, the polar region of ligands **1**, **2**, and **3** near the endoperoxide bridge is directed towards the Fe^{2+} ion of transferrin. For ligand **1** (IC_{50} = 97.0 µM), the d(O1Fe^{2+}) and d(O2Fe^{2+}) distances are 2.10 and 2.91 Å (ELL = -4.60 kcal/mol), respectively, while these distances in ligands **2** (IC_{50} = 0.46 µM) and **3** (IC_{50} = 0.79 µM) are d(O1Fe^{2+}) = 4.44 and d(O2Fe^{2+}) = 4.83 Å (ELL = -5.14 kcal/mol); d(O1Fe^{2+}) = 3.01 and d(O2Fe^{2+}) = 3.56 Å (ELL = -4.54 kcal/mol), respectively. For ligand **4** (IC50 > 100 µM), the remaining O atom of the endoperoxide bridge is shown to be directed to the Fe^{+2} ion of transferrin with the d(OFe^{2+}) = distance being punctuated at 2.47 Å (ELL = -3.39 kcal/mol).

Figure 7 shows the interactions of ligands **1**, **2**, **3**, and **4** with the heme receptor. As can be seen in this figure, the polar region of the ligand, close to the endoperoxide bridge, C3-O1-O2-C12a, is directed towards the Fe^{2+} ion of heme, with ligands **1**, **2**, **3,** and **4** distant from the Fe^{2+} ion of heme as follows: ligand **1** (IC_{50} = 97.0 µM), d(O1Fe^{2+}) and d(O2Fe^{2+}) = 2.61 and 3.66 Å (ELL = -6.53 kcal/mol), respectively; ligand **2** (IC_{50} = 0.46 mM), d(O1Fe^{2+}) and d(O2Fe^{2+}) = 2.33 and 3.30 Å (ELL = -7.40 kcal/mol, respectively; ligand **3** (IC_{50} = 0.79 mM), d(O1Fe^{2+}) and d(O2Fe^{2+}) = 2.42 and 3.42 Å (ELL = -7.32 kcal/mol), respectively; and ligand 4 (IC_{50} > 100 mM), d(OFe^{2+}) = 3.27Å.

Based on the investigation with molecular docking, it can be reported that the interactions between ligands **1**, **2**, **3** and **4** and transferrin and heme receptors highlight relevant points: (1) artemisinin and derivatives **1**, **2** and **3**, due to the existence of the endoperoxide bridge, C3-O1-O2-C12a, exhibit activities against HepG2 cancer, with the O1 atom being closer to the Fe^{2+} ion in the ligand-receptor interaction. Furthermore, it can be noted that the aforementioned distances in the interaction with the transferrin receptor behave in increasing order from the most active ligand to the least active, namely: d(O1Fe^{2+}) and d(O2Fe^{2+}) in ligand **2** > d(O1Fe^{2+}) and d(O2Fe^{2+}) in ligand **3** > d(O1Fe^{2+}) and d(O2Fe^{2+}) in ligand **1**, showing the inverse occurrence in the interaction with the heme receptor, that is: d(O1Fe^{2+}) and d(O2Fe^{2+}) in ligand **2** < d(O1Fe^{2+}) and d(O2Fe^{2+}) in ligand **3** < d(O1Fe^{2+}) and d(O2Fe^{2+}) in ligand **1**. The evidence described in this experiment is likely justified by the distinct situations that occur in interactions with

transferrin and heme receptors. According to the literature, circulating iron is captured by transferrin (holotransferrin protein) and transported to the tumor cell (Andrews, 2000). Artemisinins form a covalent bond with transferrin and are also transported to the cancer cell. When iron transported by holotransferrin is released inside this cell, it interacts with artemisinins to form free radicals that cause cell death (Lai *et al.,* 2006). According to the literature, when artemisinins are administered targeting mitochondria, the interaction with heme Fe^{2+} is immediate (Dan-Dan *et al.,* 2025). In both situations, ligand-Fe^{2+} ion (transferrin) and ligand-Fe^{2+} ion (heme), according to the interaction distances reported in this investigation, the distances between the oxygen atoms of the endoperoxide bridge and Fe^{2+} (heme) are smaller than those presented in the interaction with Fe^{2+} ions (transferrin). Furthermore, in the ligand-transferrin interaction, the most active artemisinins exhibit greater interaction distances with Fe^{2+}, while in the ligand-heme interaction the most active artemisinins exhibit smaller interaction distances with the receptor; (2) ligand **4**, due to the loss of the aforementioned bridge, behaves practically as an inactive molecule against HepG2 cancer; (3) it is important to emphasize that the investigation shows that the trioxane ring is crucial for the activity of artemisinin (**1**) and derivatives (**2** and **3**) against HepG2 cancer, and this activity is probably potentiated by the lipophilic property of the molecules due to the large number of atoms present in them (Barbosa *et al.,* 2007); (**4**) finally, the histidine unit in heme generally coordinates to Fe^{2+} through its sp^2 N atom, which allows the iron ion to acquire a hexacoordinated octahedral arrangement after binding to artemisinin (**1**) and derivatives (**2** and **3**) (Costa *et al.,* 2007; Haynes & Vonwiller, 1996).

5 CONCLUDING REMARKS

B3LYP/6-31G** comprised the theoretical method/basic set suitable for investigating the cruciality of the 1, 2, 4-trioxane ring in the anticancer artemisinin activities due to the improved 3D structure description of artemisinin (**1**). By elucidating the structure-activity relationship (SAR) of ligands (**1** to **4**), it can be reported that MEP proved to be a tool capable of avoiding the selection of inactive compounds in the design stage of new potentially active derivatives against HepG2 cancer, reinforcing the

importance of the 1, 2, 4-trioxane ring in the design of active derivatives. Furthermore, molecular docking also indicated the relevance of the 1, 2, 4-trioxane ring for the design of artemisins active against cancer. In addition, the literature reports the descriptor $\varepsilon_{LUMO} - \varepsilon_{HOMO}$ as relevant in the biological process of artemisinin and transferrin receptor interaction (Barbosa *et al., 2011*), therefore, it is relevant to understand the procedure involved when addressing the topic. Finally, the experiment developed can be used as an exercise to accumulate the systematic investigation proposed at different levels of Chemistry Education.

ACKNOLEDGMENTS

The authors thank LQTC-Faqui-UFPA and LSP-IFPA-Campus de Castanhal for their computer support and IASA-São Luís (MA), IFPA-Campus de Castanhal, and LQTC-Faqui-UFPA for their help in preparing the manuscript.

There are no conflicts of interest.

6 REFERENCES

Allen, F. H. (2002). The Cambridge Structural Database: a quarter of a million crystal structures and rising. Acta Crystallography B58, 380-388. https://doi.org/ 10.1107/s0108768102003890

Andrews, N. C. (2000). Iron homeostasis: Insights from genetics and animal models. Nature Review 1, 208–217. https://doi.org/10.1038/35042073

Araújo, J. J. O., Miranda, R. M., Castro, J. S. O., de Figueiredo, A. F., Pinheiro, A. C. B., Morais, S. S. S., dos Santos, M. A. B., Pinheiro, A. L. R., Gil, F. S., Bitencourt, H. R., Alves, G. H. R., & Pinheiro, J. C. (2022). Designing Artemisinins with Antimalarial Potential, Combining Molecular Electrostatic Potential, Ligand-heme Interaction and Multivariate Models. Computational Chemistry, 11(1), 1-23. utational Chemistry, 2023, 11, 1-23 https://www.scirp.org/journal/cc

Avery, M. A., Muraleedharan, K. M., Desai, P. V., Bandyopadhyaya, A. K., Furtado, M. M., & Tekwan, B. L. (2003). Structure-Activity Relationships of the Antimalarial Agent Artemisinin. 8. Design, Synthesis, and CoMFA Studies toward the Development of Artemisinin-Based Drugs against Leishmaniasis and Malaria. Journal of Medicinal Chemistry 46 (20), 4244-4258. https://doi.org/10.1021/jm030181q

Barbosa, P. J., Ferreira, J. E. V., de Figueiredo, A. F., de Almeida, R. C. O., Silva, O. P. P. S.,

Carvalho, R. J. C., Cristino, M. G. G., Ciríaco-Pinheiro, J., Vieira, J. L. F., & Serra, R. T. A. (2011). Molecular modeling and chemometric study of anticancer derivatives of artemisinin. Journal of Serbian Chemica Society, 76(9), 1263–1282. https://doi.org/ 10.2298/JSC111227111B

Becke, A. D. (1993). Density-functional thermochemistry. III. The role of exact exchange. Journal of Chemical Physics, 98(7), 5648-5652. https://doi.org/10.1063/1.464913
Blinder, S. M. (1965). Basic Concepts of Self-Consistent-Field Theory. American Journal of Physics, 33(6), 431-443. https://doi.org/10.1119/1.1971665
Bray, F., Laversanne, M., Sung, H., Ferlay, J., Siegel, R. L., Soerjomataram, I., & Jemal, J. (2024). Global cancer statistics 2022: GLOBOCAN estimates of incidence and mortality worldwide for 36 cancers in 185 countries. CA: A Cancer Journal for Clinicians, 74, 229–263. https:// doi.org/ 10.3322/caac.21834
Cardoso, F. J. B., de Figueiredo, A. F., Lobato, M. S., de Miranda, R. M., de Almeida, R. C. O., & Pinheiro, J. C. (2008). A study on antimalarial artemisinin derivatives using MEP maps and multivariate QSAR, Journal of Molecular Modeling 14 (1), 39–48. https://doi.org/10.1007/s00894-007-0249-9

Castro, J. S. O., Pinheiro, J. C., Morais, S. S. S., Bitencourt, H. R., de Figueiredo, A. F., dos Santos, M. A. B., Gil, F. S., & Pinheiro, A. C. B. (2023). Design of N-11-Azaartemisinins Potentially Active against Plasmodium falciparum by Combined Molecular Electrostatic Potential, LigandReceptor Interaction and Models Built with Supervised Machine Learning Methods. Journal of Biophysical Chemistry, 14(1), 1-29. https://www.scirp.org/journal/jbpc

Chen, H. H., Zhou, H. J., & Fang, X. (2003). Inhibition of human cancer cell line growth and human umbilical vein endothelial cell angiogenesis by artemisinin derivatives in vitro. Pharmacological Research 48 (3), 231-236. https://doi.org/10.1016/S1043-6618(03)00107-5

Costa, M. S., Kiralj, R., & Ferreira, M. M. C. (2007). Estudo Teórico da Interação Existente Entre a Artemisinina e o Heme Químca Nova, 30 (1), 25-31.

Dan-Dan, W., Li, H., Ming-Hui, Q., Hong-Yang, Z., Ai-Xi, Y., & Shi-Wen, H. (2025). Mitochondria-targeting artesunate-rhein conjugates: Linker-modulated cell-permeability, heme-affinity and anticancer activity. European Journal of Medicinal Chemistry 282 117100. https://doi.org/10.1016/j.ejmech.2024.117100

Dewar, M. J. S., & Kelemen, J. (1971). LCAO MO Theory Illustrated by Its Application to H2. Journal of Chemical Education, 48(8), 499-501. https://doi.org/10.1021/ed048p494

Dewar, M. J. S., Zoebisch, E. G., Healy, E. F., & Stewart, J. J. P. (1985) Development and use of quantum mechanical molecular models. 76. AMI: a new general purpose quantum mechanical molecular model. Journal of the American Chemical Society, 107(13), 3902-3909. https://doi.org/10.1021/ja00299a024

Efferth, T., Dunstan, H., Sauerbrey, A., Miyachi, H., & Chitambar, C. R. (2001). The anti-

malarial artesunate is also active against cancer. International Journal of Oncology 18 (4), 767-73. https://doi.org/10.3892/ijo.18.4.767

Efferth, T., Rauh, R., Kahl, S., Tomicic, M., Böchzelt, H., Tome, M. E., Briehl, M. M., Bauer, R., & Kaina, B. (2005). Molecular modes of action of cantharidin in tumor cells. Biochemical Pharmacology, 69 (5), 811-188. https://doi.org/doi: 10.1016/j.bcp.2004.12.003

Frisch, M. J., Trucks, G. W., Schlegel, H. B., Scuseria, G. E., Robb, M. A., Cheeseman, J. R., Montgomery, J. A., Vreven, T., Kudin, K. N., Burant, J. C., Millam, J. M., Iyengar, S. S., Tomasi, J., Barone, V., Mennucci, B., Cossi, M., Scalmani, G., Rega, N., Petersson, G. A., Nakatsuji, H., Hada, M., Ehara, M., Toyota, K., Fukuda, R., Hasegawa, J., Ishida, M., Nakajima, T., Honda, Y., Kitao, O., Nakai, H., Klene, M., Li, X., Knox, J. E., Hratchian, H. P., Cross, J. B., Bakken, V., Adamo, C., Jaramillo, J., Gomperts, R., Stratmann, R. E., Yazyev, O., Austin, A. J., Cammi, R., Pomelli, C., Ochterski, J. W., Ayala, P. Y., Morokuma, K., Voth, G. A., Salvador, P., Dannenberg, J. J., Zakrzewski, V. G., Dapprich, S., Daniels, A. D., Strain, M. C., Farkas, O., Malick, D. K., Rabuck, A. D., Raghavachari, K., Foresman, J. B., Ortiz, J. V., Cui, O., Baboul, A. G., Clifford, S., Cioslowski, J., Stefanov, B. B., Liu, G., Liashenko, A., Piskorz, P., Komaromi, I., Martin, R. L., Fox, D. J., Keith, T., Al-laham, M. A., Peng, C. Y., Nanayakkara, A., Challacombe, M., Gill, P. M. W., Johnson, B., Chen, W., Wong, M. W., Gonzalez, C., & Pople, J. A. (1998). Gaussian 98, Revision A.6. Gaussian, Inc., Pittsburgh.

Flukiger, P., Luthi, H. P., Portmann, S., & Weber. J. (2000-2001). Molekel. Swiss Center for Scientific Computing: Mano, Switzerland.

Guo, W., Wang, W., Lei, F., Zheng, R., Zhao, X., Gu, Y., Yang, M., Tong, Y., & Wang, Y. (2024). Identifying the Main Components and Mechanisms of Action of *Artemisia annua* L. in the Treatment of Endometrial Cancer Using Network Pharmacology. ACS Omega 9, 8055-8066. https://doi.org/10.1021/acsomega.3c08320

Goodsell, D. S., Morris, G. M., & Olson, A. J. (1996). Automated Docking of Flexible Ligands: Applications of AutoDock. Journal of Molecular Recognition, 9(1), 1-5. https://doi.org/10.1002/(sici)1099-1352(199601)9:1<1::aid-jmr241>3.0.co;2-6

Haber, D. A., & Fearon, E. R. (1998). The promise of cancer genetics. The Lancet, 351, SII1-SII8. https://doi.org/10.1016/s0140-6736(98)90326-9

Haynes, R. K., & Vonwiller, S. C. (1996) The behaviour of qinghaosu (artemisinin) in the presence of heme iron (II) and (III). Tetrahedron Letters, 37 (2), 253-256. https://doi.org/10.1016/0040-4039(95)02141-8

Hehre, W. J., Radom, L., Schleyer, P.v. R., & Pople, J. A. (1986). Ab Initio Molecular Theory. Wiley, New York.

HyperChem, Inc. (2008) ChemPlus: Modular Extension to HyperChem Realease 8.06. Molecular Modeling for Windows. Gainesville.

Jana, S., Iram, S., Thomas, J., Liekens, S., & Dehaen, W. (2017). Synthesis and anticancer activity of novel aza-artemisinin derivatives. Bioorganic & Medicinal Chemistry 3671–3676. http://dx.doi.org/10.1016/j.bmc.2017.04.04

Khanal, P. (2021). Antimalarial and anticancer properties of artesunate and other artemisinins: current development. Monatshefte für Chemie - Chemical Monthly 152, 387–400. https://doi.org/10.1007/s00706-021-02759-x

Lai, H. C., Sasaki, T., & Singh, N. P. (2004). Covalent conjugates between artemisinin related endoperoxides and iron-carrying proteins and methods of use. Patent Application Publication, Pub. No.: US200/0067875A1

Leban, I., Golic, L., & Japelj, M. (1988). Crystal and molecular structure of Qinghaosu: a redetermination, Acta Pharmaeutica Jugoslavica 38, 71-77

Lee, C., Yang, W., & Parr, R. G. (1988). Development of the colic-salvetti correlation-energy formula into a functional of the electron density. Physical Review B, 37(2), 785-789. https://doi.org/10.1103/PhysRevB.37.785

Lisgarten, J. N., Potter, B. S., Bantuzerko, C., & Palmer, R. A. (1988). Structure, absolute configuration, and conformation of the antimalarial compound: Artemisinin. Jounal of Chemical Crystallography, 28, 539-543. https://doi.org/10.1023/A:1023244122450

Liu, Y., Wong, V. K.-W., Ko, B. C.-B., Wong, M.-K., & Che, C.-M. (2005). Synthesis and Cytotoxicity Studies of Artemisinin Derivatives Containing Lipophilic Alkyl Carbon Chains. Organic Letters 7 (8), 1561-1564. https://doi.org/10.1021/ol050230o

Ma, Z., Woon, C. Y.-N., Liu, C.-G., Cheng, J.-T., You, M., Sethi, G., Wong, A. L.-A., Ho, P. C.-L., Zhang, D., Ong, P., Wang, L., & Goh, B.-C. (2021). Repurposing Artemisinin and its Derivatives as Anticancer Drugs: A Chance or Challenge? Frontiers in Pharmacology 12, 828856. https://doi.org/10.3389/fphar.2021.828856

MacGillivray, R. T. A., Moore, A. S., Chen, J., Anderson, B. F., Baker, H., Luo, Y., Bewley, M., Smith, C. A., Murphy, M. E. P., Wang, Y., Mason, A. B., Woodworth, R. C., Brayer, G. D., & Baker,| E. M. (1988). Two High-Resolution Crystal Structures of the Recombinant N-Lobe of Human Transferrin Reveal a Structural Change Implicated in Iron Release. Biochemistry, 37, 7919-7928. https://doi.org/10.1021/bi980355j

Meng, E. C., Goddard, T. D., Pettersen, E. F., Couch, G. S., Pearson, Z. J., Morris, J. H., & Ferrin, T. E. (2023). UCSF ChimeraX: Tools for structure building and analysis. Protein Science 32 (11), e4792. https://doi.org/10.1002/pro.4792

O'Boyle, N. M., Banck, M., James, C. A., Morley, C., Vandermeersch, T., & Hutchison, G. R. (2011) Open Babel: an open chemical toolbox. Journal of Cheminformatics, 3(33), 1-14. https://doi.org/10.1186/1758-2946-3-33

Oliveira , L. F. S., Cordeiro, H. C., Brito, H. G., Pinheiro, A. C. B., dos Santos, M. A. B., Bitencourt, H. R., de Figueiredo, A. F., Araújo, J. J. O., Gil, F. S., Farias, M. S., Barbosa, J. P., & Pinheiro, J. C. (2021). Molecular electrostatic potential and pattern recognition models to design potentially active pentamidine derivatives against Trypanosoma brucei rhodesiense. Research Society and Development, 10(12), e261101220207. https://doi.org/10.33448/rsd-v10i12.20207

O'Neill, P. M., Barton, V. E., & Ward, S. A. (2010). The Molecular Mechanism of Action of Artemisinin—The Debate Continues. Molecules, 15,1705 – 1721. https://doi.org/ 10.3390/molecules15031705

Opsenica, D. M., & Solaja, B. A. (2009). Antimalarial peroxides. Journal Serbian Chemical Society 74, 1155-1193. https://doi.org/doi: 10.2298/JSC0911155O

Pizon, M. D. G., Farias, M. S., de Figueiredo, A. F., Gil, F. S., Pinheiro, A. C. B., Pinheiro, A. L. R., dos Santos, M. A. B., & Pinheiro, J. C. (2024). Relevance of the 1,2,4-trioxane ring in the leishmanicidal activity of artemisinin and derivatives: a computational study. African Journal of Chemical Education, 14(3), 141–158. https://www.ajol.info/index.php/ajce/article/view/276637

Politzer, P., Laurence, P., & Jayasuriya, K. (1985). Molecular Electrostatic Potentials: An Effective Tool for the Elucidation of Biochemical Phenomena. Environmental Health Perspectives, 61, 191-202. https://doi.or/10.1289/ehp.8561191

Politzer, P., Murray, J. (2021). The Neglected Nuclei. Molecules, 26(10) 2982. https://doi.org/10.3390/molecules26102982

Politzer, P., & Truhlar G (1981). Chemical Applications of Atomic and Molecular Electrostatic Potentials. Plenum Press: New York.

Pople, J. A., & Beveride, D. L. (1970). Approximate Molecular Orbital Theory. McGraw-HilL, New York.

Price, R., Luxemburger, C., van Vugt, M., Nosten, F., Kham, A., Simpson J., Looareesuwan, S., Chongsuphajaisiddhi, T., & White, N. J. (1998). Artesunate and mefloquine in the treatment of uncomplicated multidrug-resistant hyperparasitaemic falciparum malaria. Transactions of the Royal Society of Tropical Medicine and Hygiene 92 (2), 207-211. https://doi.org/10.1016/S0035-9203(98)90750-7

Protein Data Bank. The Rutgers State University. Piscataway, New Jersey. http:www.resb.org/pdb/

Rinner, B., Siegl, V., Pürstner, P., Efferth, T., Brem, B., Greger, H., & Pfragner, R. (2004). Activity of Novel Plant Extracts Against Medullary Thyroid Carcinoma Cells. Anticancer Research, 24, 495-500.

Roothaan, C. C. J. (1951). New Developments in Molecular Orbital Theory. Reviews of

Modern Physics 23(2), 69-89. https://doi.org/10.1103/RevModPhys.23.69

Rosenberg, A. S. (2001). Progress in human tumour immunology and immunotherapy. Nature, 411, 380–384. https://doi.org/10.1038/35077246

Sasaki, T., Lai, H. C.-Y., Singh, N. P., & Oh, S. J (2007) University of Washington. US2007//0231300A1.

Schaftenaar, G., & Noordik, J. H. (2000) Molden: a pre-and post processing program for molecular and electronic structures. Journal of Comput-Aided Molecular Design, 14, 123-134. https://doi.org/10.1023/A:1008193805436

Stanzione, F., Giangreco, I., & Cole, J. C. (2021). Use of molecular docking computational tools in drug discovery. In: Witty DR, Cox B, Eds, Progress in Medicinal Chemistry. Elsevier: New York.

Thomsen, R. (2003). Flexible ligand docking using evolutionary algorithms: investigating the effects of variation operators and local search hybrids. Biosystems, 72 (1-2), 57-73. https://doi.org/10.1016/S0303-2647(03)00135-7

Vojtechovský, J., Chu, K., Berendzen, J., Sweet, R. M., & Schlichting, I. (1999). Crystal Structures of Myoglobin-Ligand Complexes at Near-Atomic Resolution. Biophysical Journal, 77, 2153-2174. https://doi.org/10.1016/S0006-3495(99)77056-6

Wall, M. E., & Wani, M. C. (1996). Camptothecin and taxol: from discovery to clinic. Journal of Ethnopharmacology 51 (1-3), 239-254. https://doi.org/doi: 10.1016/0378-8741(95)01367-9

Wani, K. I., Choudhary, S., Zehra, A., Naeem, M., Weathers, P., & Aftab, T. (2021). Enhancing artemisinin content in and delivery from *Artemisia annua:* a review of alternative, classical, and transgenic approaches. Planta 254, 29. https://doi.org/10.1007/s00425-021-03676-3

Wen, L., Chan, B., C.-L., Qiu, M.-H., Leung, P.-C., & Wong, C.-K. (2024). Artemisinin and Its Derivatives as Potential Anticancer Agents. *Molecules 29,* 3886. https:// doi.org/10.3390/molecules29163886

Wu, X., Thiel, W., Pezeshki, S., & Lin, H. (2013). Specific Reaction Path Hamiltonian for Proton Transfer in Water: Reparameterized Semiempirical Models. Journal of Chemical Theory and Computation, 9(6), 2672-2686. https://doi.org/10.1021/ct400224n

Xu, C., Zhang, H., Um, L., & Yang, X. (2020). Artemisinins as Anticancer Drugs: Novel Therapeutic Approaches, Molecular Mechanisms, and Clinical Trials. Frontiers in Pharmacology 11, 529881. https://doi.org/10.3389/fphar.2020.529881